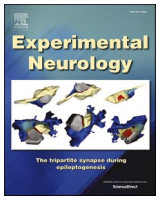
Experimental Neurology 380 (2024) 114914



Contents lists available at ScienceDirect

Experimental Neurology

journal homepage: www.elsevier.com/locate/yexnr



Research paper



Investigating therapeutic nonsense suppression in a neurofibromatosis mouse model

Chan Wu [a], Mohammed Salman Shazeeb [b], Kotchaphorn Mangkalaphiban [c], George Han [b,e], Ahmet Peker [b,f], Zubir S. Rentiya [b,g], Matthew J. Gounis [b], Allan Jacobson [a,d,*]

[a] Department of Microbiology, UMass Chan Medical School, Worcester, MA, USA
[b] Department of Radiology, UMass Chan Medical School, Worcester, MA, USA
[c] Department of Genomics and Computational Biology, UMass Chan Medical School, Worcester, MA, USA
[d] Li Weibo Institute for Rare Disease Research, UMass Chan Medical School, Worcester, MA, USA
[e] Department of Medicine, Beth Israel Deaconess Medical Center, Brockton, MA, USA
[f] Koç University Hospital, Istanbul, Türkiye
[g] Department of Radiation Oncology & Radiology, University of Virginia, Charlottesville, VA, USA

ARTICLE INFO

Keywords:
Ataluren
Neurofibromatosis
Plexiform neurofibromas
Patient-derived *Nf1* mouse model
Sex factors in NF1

ABSTRACT

Neurofibromatosis type 1 (NF1) is a human genetic disorder caused by variants in the *NF1* gene. Plexiform neurofibromas, one of many NF1 manifestations, are benign peripheral nerve sheath tumors occurring in up to 50% of NF1 patients. A substantial fraction of *NF1* pathogenetic variants are nonsense mutations, which result in the synthesis of truncated non-functional NF1 protein (neurofibromin). To date, no therapeutics have restored neurofibromin expression or addressed the consequences of this protein's absence in NF1 nonsense mutation patients, but nonsense suppression is a potential approach to the problem. Ataluren is a small molecule drug that has been shown to stimulate functional nonsense codon readthrough in several models of nonsense mutation diseases, as well as in Duchenne muscular dystrophy patients. To test ataluren's potential applicability in nonsense mutation NF1 patients, we evaluated its therapeutic effects using three treatment regimens in a previously established NF1 patient-derived (c.2041C > T; p.Arg681X) nonsense mutation mouse model. Collectively, our experiments indicate that: i) ataluren appeared to slow the growth of neurofibromas and alleviate some paralysis phenotypes, ii) female *Nf1*-nonsense mutation mice manifested more severe paralysis and neurofibroma phenotypes than male mice, iii) ataluren doses with apparent effectiveness were lower in female mice than in male mice, and iv) age factors also influenced ataluren's effectiveness.

1. Introduction

Neurofibromatosis type 1 (NF1) is one of the most common human genetic diseases, affecting approximately 1 in 3000 individuals globally (Friedman, 1999). NF1 patients exhibit a wide range of manifestations, with common symptoms including pigmentary abnormalities (Café-au-lait macules, skinfold freckling, and Lisch nodules), development of benign and malignant tumors in the peripheral and central nervous systems (neurofibromas, malignant peripheral nerve sheath tumors, and gliomas), skeletal deformities, and cognitive deficits (Cimino and Gutmann, 2018). Notably, the presence of neurofibromas is the most common NF1 manifestation. Almost all patients develop benign cutaneous and subcutaneous neurofibromas by adulthood, and up to 50% of NF1 patients develop plexiform neurofibromas (PNFs) (Mautner et al., 2008; Plotkin et al., 2012; Rasmussen and Friedman, 2000). PNFs are congenital and benign tumors that grow slowly along multiple nerve fascicles, resulting in a diffuse mass of thickened nerves either internally or on the surface of the body. Although benign, some PNFs can grow into large and bulky tumors compressing surrounding tissues and structures, causing substantial morbidities including pain, motor dysfunction, neurologic deficits, disfigurement, orthopedic symptoms, and airway difficulties (Gross et al., 2018; Prada et al., 2012). PNFs also have ~10% lifetime risk of transforming into malignant peripheral nerve sheath tumors (MPNSTs), malignancies that are the principal cause of death in NF1 patients (Evans et al., 2002).

NF1 is a large gene located on chromosome 17q11.2 that encodes

* Corresponding author at: Department of Microbiology, UMass Chan Medical School, Worcester, MA, USA.
E-mail address: allan.jacobson@umassmed.edu (A. Jacobson).

https://doi.org/10.1016/j.expneurol.2024.114914
Received 1 April 2024; Received in revised form 15 July 2024; Accepted 31 July 2024
Available online 4 August 2024
0014-4886/© 2024 The Authors. Published by Elsevier Inc. This is an open access article under the CC BY-NC license (http://creativecommons.org/licenses/by-nc/4.0/).

neurofibromin, a protein that functions as a tumor suppressor (DeClue et al., 1991; Gutmann et al., 1991; Xu et al., 1990). Almost 3000 *NF1* pathogenic variants have been reported, of which ~15–20% are nonsense mutations (Gutmann et al., 2017; Philpott et al., 2017; Stenson et al., 2020). Such mutations encode premature termination codons (PTCs) in *NF1* mRNA and, as a consequence, severely reduce neurofibromin production by leading to the synthesis of truncated, non-functional neurofibromin and by activating nonsense-mediated mRNA decay (NMD) of the *NF1* transcript (Anastasaki et al., 2017; Bashyam, 2009; Brinckmann et al., 2007; He and Jacobson, 2015; Miller and Pearce, 2014; Osborn and Upadhyaya, 1999). Therapeutic nonsense suppression is an approach to treating diseases caused by nonsense mutations that employs small molecule drugs, or other pharmaceuticals, to enhance PTC readthrough and produce full-length protein from mRNAs that otherwise lack a complete open reading frame (Keeling et al., 2014; Leier et al., 2020; Peltz et al., 2013). Ataluren is a safe, orally bioavailable small molecule drug that has been employed for therapeutic nonsense suppression. It stimulates functional readthrough of nonsense-containing mRNAs (Keeling et al., 2014; Peltz et al., 2009; Roy et al., 2016; Roy et al., 2015; Welch et al., 2007), promotes functional readthrough of the codon 683 PTC of mouse *Nf1* mRNA (a mouse counterpart of the human *NF1* nonsense mutation in exon 18, c.2041C > T; p.Arg681X (Wu et al., 2022)), and has been employed as a therapeutic for nonsense mutation Duchenne muscular dystrophy patients (McDonald et al., 2017; McDonald et al., 2013; Mercuri et al., 2023).

To evaluate ataluren's potential for therapeutic efficacy in NF1, we assessed its effects in *Dhh-Cre; Nf1*$^{R683X/4F}$ mice, a previously established NF1 patient-derived nonsense mutation mouse model (Li et al., 2016). In this model, mice develop neurofibromas along the spinal column, which compress the spinal cord and lead to paralysis. We treated these mice by feeding them chows infused with different levels of ataluren, commencing at different ages. In parallel, additional *Dhh-Cre; Nf1*$^{R683X/4F}$ mice were injected with clitocine, a nucleoside analog that also induces readthrough of nonsense mutations but which is less desirable as a therapeutic agent because it is not orally available and can be toxic at elevated doses (Friesen et al., 2017). Our experiments demonstrated that: a) female *Dhh-Cre; Nf1*$^{R683X/4F}$ mice showed more severe phenotypes than male *Dhh-Cre; Nf1*$^{R683X/4F}$ mice of similar ages, b) ataluren, but not clitocine, slowed the growth of neurofibromas and alleviated paralysis phenotypes, c) the dosing and timing of treatment affected the efficiency of ataluren treatment, and d) although some of our results lack statistical significance, the overall therapeutic trends are clear.

2. Results

2.1. Sex disparities in phenotypic severity of *Dhh-Cre; Nf1*$^{R683X/4F}$ mice

The *Nf1* mouse model of *Dhh-Cre; Nf1*$^{R683X/4F}$ containing a variant recapitulating human variant c.2041C > T; p.Arg681X was established previously (Li et al., 2016). These mice were reported to develop paralysis at ~four months of age, exhibit weight loss, and form neurofibromas around dorsal root ganglia (DRG) or nerve roots along the spinal cord (Li et al., 2016). However, whether sex affects the penetrance of related symptoms has never been evaluated. To determine whether sex is a risk factor, we bred the *Nf1*$^{R683X/4F}$ mice with *Dhh-Cre* mice to generate *Dhh-Cre; Nf1*$^{R683X/4F}$ mice (Fig. 1A) and maintained the offspring for 5 months to assess the phenotypes of both female and male mice.

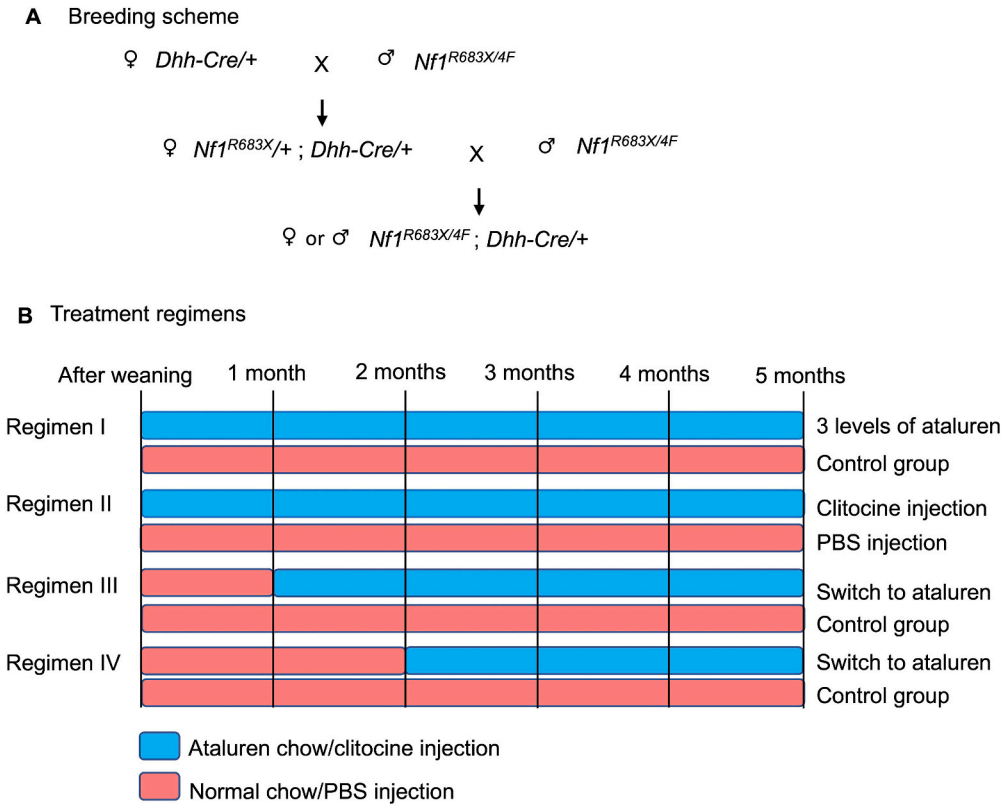


Fig. 1. Nonsense suppression treatment strategy in an NF1 patient-derived mouse model. (A) Breeding scheme for the generation of *Dhh-Cre; Nf1*$^{R683X/4F}$ mice. (B) Ataluren or clitocine treatment regimens. For ataluren treatment, mice were fed ataluren infused chow from after weaning (Regimen I), one month after weaning (Regimen III), and two months after weaning (Regimen IV), and were analyzed for tumor burden at five months after weaning. Weight and paralysis state were assessed weekly beginning immediately after weaning. Ataluren (0.03%, 0.1%, or 0.3% infusion in chow) or clitocine (subcutaneous biweekly injection of 1 mg/kg or 5 mg/kg clitocine from after weaning – see Regimen II) were tested in both male and female mice. *Dhh-Cre; Nf1*$^{R683X/4F}$ mice on normal food or injected with PBS comprised the respective no treatment controls.

At the time of birth and weaning, both female and male *Dhh-Cre; Nf1*$^{R683X/4F}$ mice were indistinguishable from their littermates, which was consistent with previous studies (Li et al., 2016). We found that female *Dhh-Cre; Nf1*$^{R683X/4F}$ mice had slightly reduced body weights compared to their female littermate controls up to 21 weeks after weaning, but the difference was not significant (Fig. 2A), whereas male *Dhh-Cre; Nf1*$^{R683X/4F}$ mice had significant weight reductions compared to the male littermate control mice of the same age (Fig. 2B). The growth curves indicated that male *Dhh-Cre; Nf1*$^{R683X/4F}$ mice developed a weight loss phenotype, but female *Dhh-Cre; Nf1*$^{R683X/4F}$ mice grew normally to 5 months.

Volumetric magnetic resonance imaging (MRI) analysis was used to quantitate tumor burden in *Dhh-Cre; Nf1*$^{R683X/4F}$ mice. As reported in a previous study (Li et al., 2016), over 90% of tumors were found in the cervical and thoracic spine and fewer than 10% of tumors were detected in the lumbar spine. However, our MRI scans indicated the presence of significantly more, and larger, tumors in female mice compared to male mice. The mean tumor number, volume, and surface area of tumors per mouse were 3.7 ± 0.4, 10.3 ± 1.7 mm^3, and 67.5 ± 9.5 mm^2 in female mice, respectively, whereas in male mice, the measurements were 2.7 ± 0.3, 5.8 ± 1.3 mm^3, and 39.1 ± 7.8 mm^2, respectively (Fig. 3A-C, normal food group). The MRI results indicated that female mice developed more severe neurofibromas than male mice of the same age.

In our MRI analyses we noticed that neurofibromas related to the cervical spine sometimes had weaker signal intensities than those related to the thoracic spine (data not shown). To validate the tumor burden analysis obtained by MRI, we performed gross dissections of *Dhh-Cre; Nf1*$^{R683X/4F}$ mice and manually measured the tumors formed in each mouse. The spinal cord with attached DRGs and nerve roots were isolated intact, and the tumors were seen along the spinal column as indicated by green arrows in Fig. 4A. We measured the largest tumor diameter perpendicular to the DRG/nerve root, and tumor perimeter as outlined by the red dashed lines (Fig. 4A). The mean tumor number by gross dissection was 4.6 ± 0.1 in females vs. 3.2 ± 0.4 in males (Fig. 4B, normal food group), the mean tumor diameter was 1.4 ± 0.04 mm in females vs. 1.2 ± 0.03 mm in males (Fig. 4C, normal food group), and the mean perimeter of tumors was 7.7 ± 0.3 mm in females vs. 7.2 ± 0.3 mm in males (Fig. 4D, normal food group). Although all three measurements of tumors were greater in female *Dhh-Cre; Nf1*$^{R683X/4F}$ mice, only the tumor number and diameter showed significant differences. When comparing the MRI measurements with dissection results, we noticed a greater variability in the metrics from MRI analysis compared to those acquired by gross dissection. This might have occurred due to the heterogeneity of neurofibroma signal intensity in the MRI images since the signal intensity, which was used as a criterion to segment tumors, was not consistent between individual neurofibromas (cervical neurofibromas vs. thoracic neurofibromas). This observation suggests that a larger sample size may be needed to increase statistical power when using MRI to compare differences in neurofibromas between groups. Nevertheless, both the MRI and gross dissection results indicated female *Dhh-Cre; Nf1*$^{R683X/4F}$ mice developed more and larger tumors than male *Dhh-Cre; Nf1*$^{R683X/4F}$ mice of the same age.

We recorded the development of the paralysis phenotype in these mice weekly and classified the degree of severity into three levels (Fig. 5). When placed in a container, normal mice were agile, had strong hindlimbs that could support their body weight to stand up freely in the container, and could climb out of the container easily. In the Paralysis I group, the mice were still agile, could stand up on hindlimbs with the support of their forelimbs against the container wall, but showed signs of paralysis in their hindlimbs. In the Paralysis II group, the mice were not active, had weak hindlimbs that could not support the body weight to stand up, and showed an obvious paralysis phenotype in their hindlimbs. In the Paralysis III group, the mice were extremely reluctant to move, remained prone most of the time, had very weak hindlimbs, and walked while dragging legs. Female *Dhh-Cre; Nf1*$^{R683X/4F}$ mice began showing signs of paralysis at week 11 after weaning, and by week 21, 61.5% (15.4% in Paralysis I, 30.7% in Paralysis II, and 15.4% in Paralysis III) of female mice developed a paralysis phenotype (Fig. 6A). Male *Dhh-Cre; Nf1*$^{R683X/4F}$ mice began showing a paralysis phenotype at week 16, and by week 21, 33.3% (26.6% in the Paralysis II group, and 6.7% in the Paralysis III group) of male mice developed a paralysis phenotype (Fig. 6E). Progression of the paralysis phenotype was slower in males compared to that in females.

Taken together, the above data showed that female mice did not show a weight loss phenotype, whereas male mice did, and female mice developed more severe neurofibromas and paralysis phenotypes than male mice.

2.2. Ataluren manifests therapeutic nonsense suppression effects in *Dhh-Cre; Nf1*$^{R683X/4F}$ mice

Since *Dhh-Cre; Nf1*$^{R683X/4F}$ mice exhibit sex disparities in the presentation of phenotypes, we tested and evaluated the nonsense suppression effects of ataluren or clitocine in both female and male *Dhh-Cre; Nf1*$^{R683X/4F}$ mice following three ataluren treatment regimens (Regimens I, III, and IV; Fig. 1B) and one clitocine treatment regimen (Regimen II; Fig. 1B).

In Regimen I, mice were fed chow infused with 0.03%, 0.1%, and

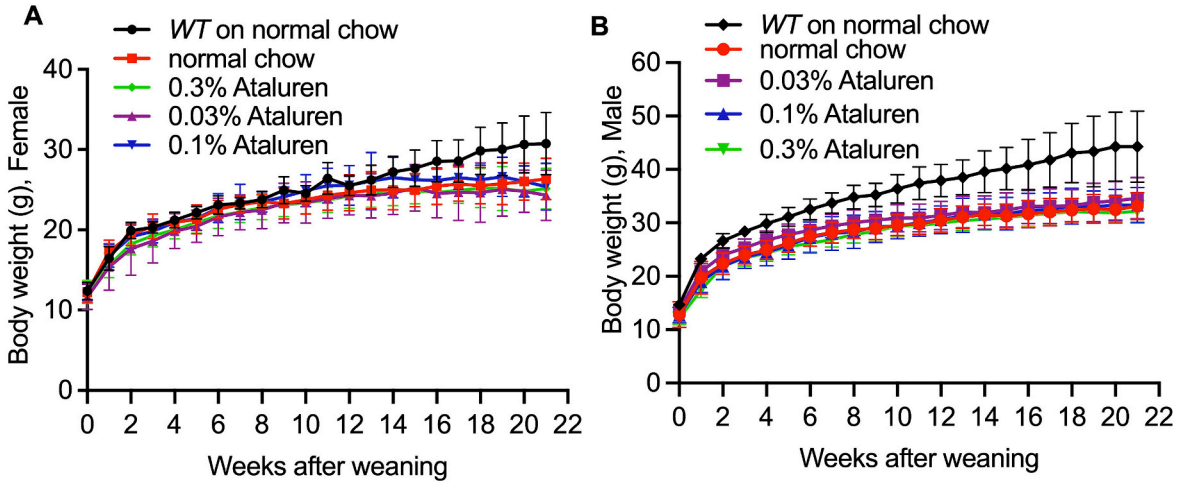


Fig. 2. Growth curves of *Dhh-Cre; Nf1*$^{R683X/4F}$ mice on Regimen I. (A) Growth curves of female *Dhh-Cre; Nf1*$^{R683X/4F}$ mice on normal chow (n = 15), 0.03% ataluren chow (n = 11), 0.1% ataluren chow (n = 11), 0.3% ataluren chow (n = 12), and siblings on normal chow (n = 8). (B) Growth curves of male *Dhh-Cre; Nf1*$^{R683X/4F}$ mice on normal chow (n = 15),

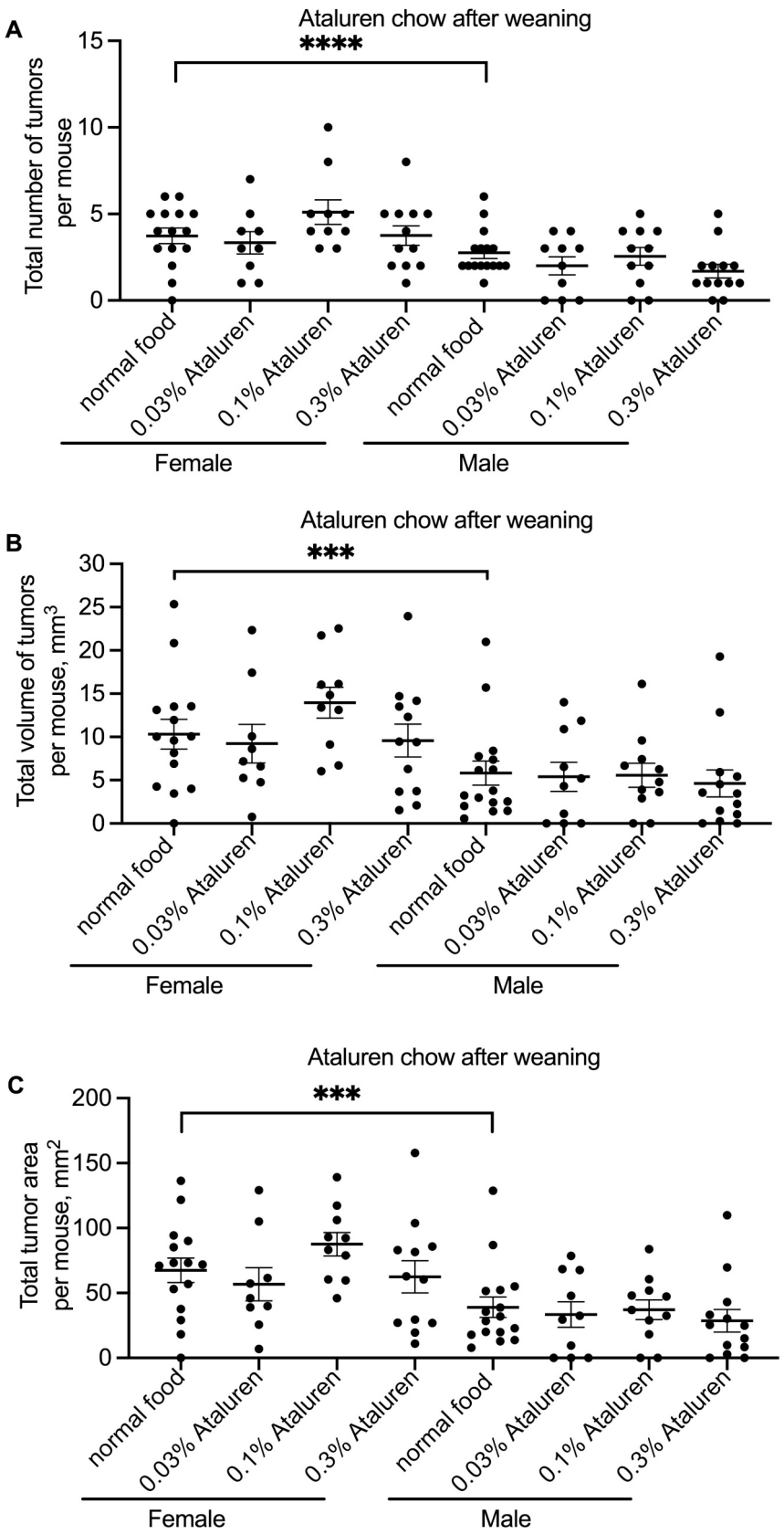


Fig. 3. Volumetric MRI analyses of *Dhh-Cre; Nf1*$^{R683X/4F}$ mice on Regimen I. The total number (A), total volume (B), and total surface area (C) of neurofibromas in individual mice on normal or ataluren chow after weaning are shown. Data are presented as mean ± SEM. *$p < 0.05$, **$p < 0.01$, ***$p < 0.001$, ****$p < 0.0001$, two-way ANOVA test with Tukey's multiple comparisons correction.

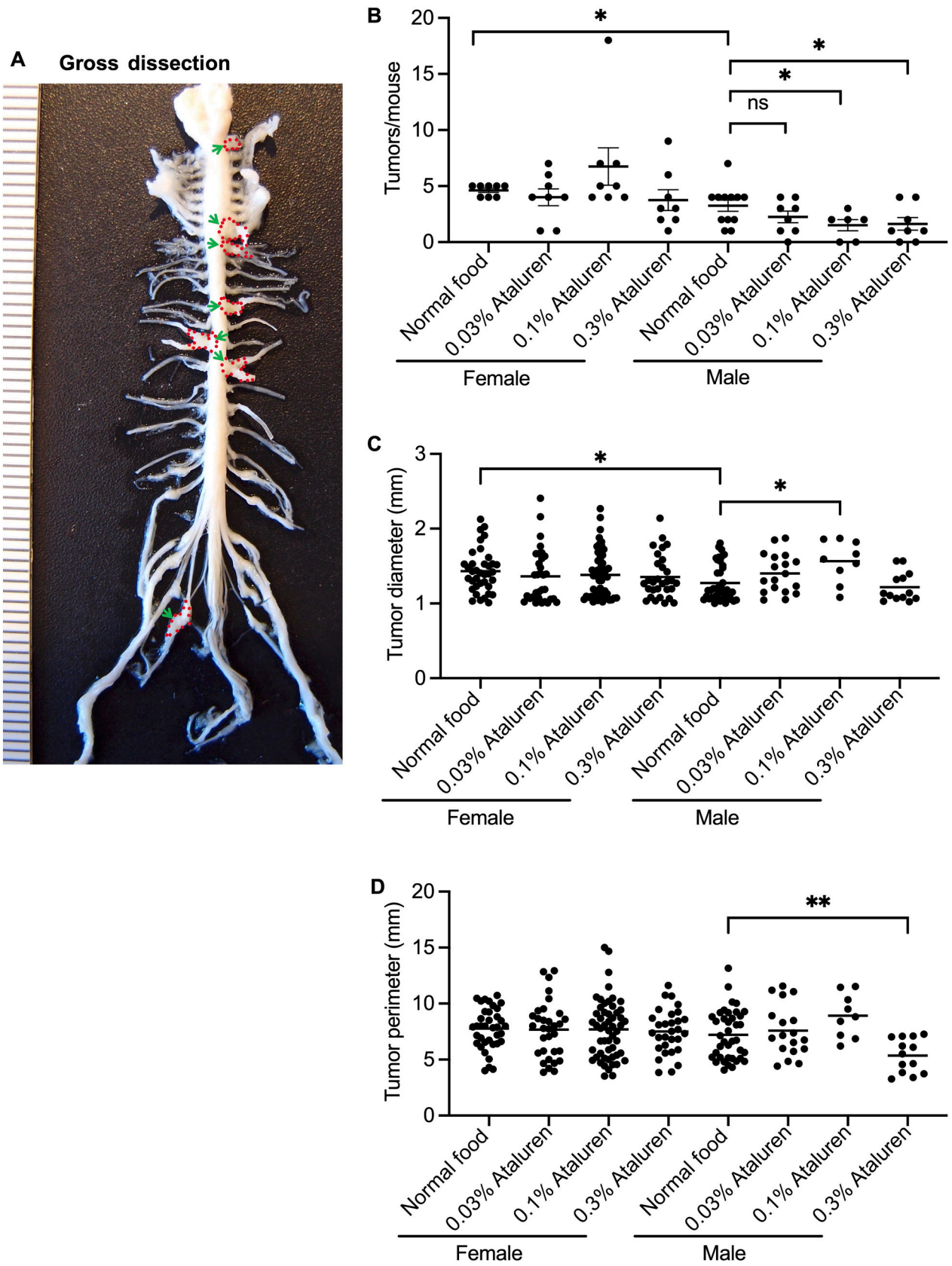


Fig. 4. Gross dissection analyses of *Dhh-Cre; Nf1*$^{R683X/4F}$ mice on Regimen I. (A) Representative image of gross dissection of *Dhh-Cre; Nf1*$^{R683X/4F}$ mouse spinal cord with attached nerves. Green arrows point to neurofibromas and dotted red lines outline their perimeters. The ruler on the left of image shows 1 mm markings. A tumor is defined as diameter >1 mm. The total tumor number per mouse (B) and the diameter (C) or perimeter (D) of the neurofibromas in mice on Regimen I are shown. Data are presented as mean ± SEM. *$p < 0.05$, **$p < 0.01$, ***$p < 0.001$, Welch's *t*-test. (For interpretation of the references to colour in this Fig. legend, the reader is referred to the web version of this article.)

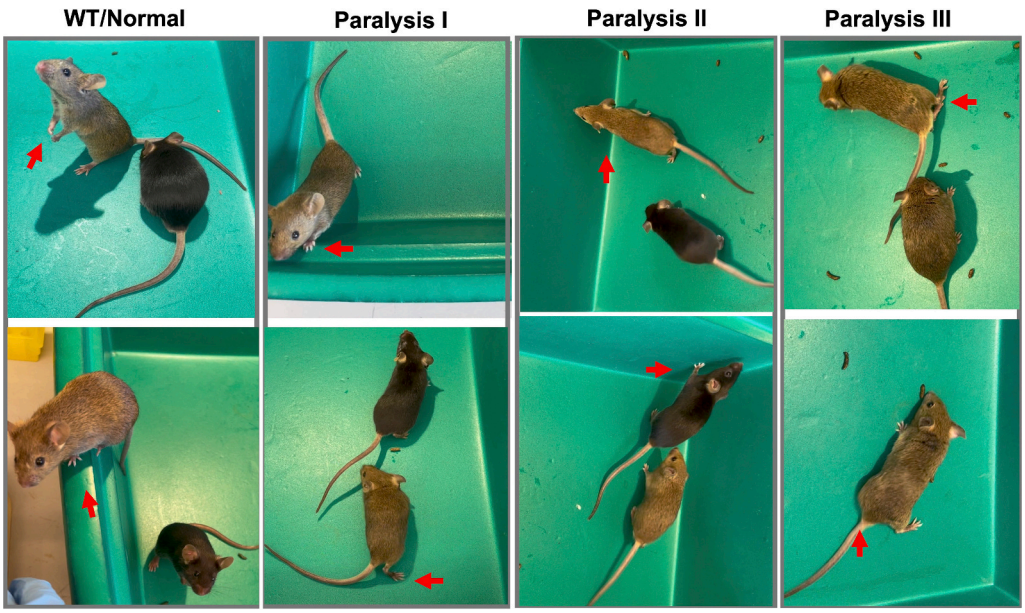


Fig. 5. Classifications of paralysis symptoms. Mice were placed in a 15"L x 12"W x 5"H container and their walking patterns were examined. Wild-type/normal group: mice ran around actively, could stand up on their hindlimbs freely, were agile, and could climb out of the container easily. Paralysis I/mild symptom group: mice were active, showed signs of paralysis on one of both of their hindlimbs, and needed support of the container wall to stand on their hindlimbs. Paralysis II/moderate symptom group: mice were not active, walked slowly, showed obvious paralysis symptoms on their hindlimbs, and could not stand on their hindlimbs. Paralysis III/severe symptom group: mice were very reluctant to move, walked with dragging legs, and had extremely weak hindlimbs. The red arrows point to the typical physical symptoms of paralyzed mice in each group. Mice were examined weekly. (For interpretation of the references to colour in this Fig. legend, the reader is referred to the web version of this article.)

0.3% ataluren chow after weaning, weighed and assessed for their paralysis phenotype weekly, imaged by MRI, and then dissected for tumor burden analyses. The body weights of female or male mice between treatment groups in this regimen showed no significant differences (Figs. 2A and B).

We first used volumetric MRI to determine whether the number, volume, and surface area of tumors were different in the ataluren treatment groups compared to the controls. In female *Dhh-Cre; Nf1*$^{R683X/4F}$ mice on 0.03%, 0.1%, and 0.3% ataluren treatment, the mean tumor numbers were 3.3 ± 0.6, 5.1 ± 0.7, and 3.7 ± 0.5, respectively (Fig. 3A); the mean tumor volumes were 9.2 ± 2.2 mm^3, 13.9 ± 1.7 mm^3, and 9.5 ± 1.9 mm^3, respectively (Fig. 3B); and the mean tumor surface areas were 56.7 ± 12.7 mm^2, 87.6 ± 8.9 mm^2, and 62.4 ± 12.3 mm^2, respectively (Fig. 3C). Compared to the normal food control group in which the mean total tumor number, volume, and surface area were 3.7 ± 0.4, 10.3 ± 1.7 mm^3, and 67.5 ± 9.5 mm^2, respectively, mice on 0.03% ataluren treatment showed some decreases, whereas mice on 0.3% ataluren treatment had similar measurements, and mice on 0.1% ataluren showed increases in all measurements. However, none of these differences between treatment groups were statistically significant.

In male *Dhh-Cre; Nf1*$^{R683X/4F}$ mice on 0.03%, 0.1%, and 0.3% ataluren treatment, the mean tumor numbers were 2 ± 0.5, 2.5 ± 0.5, and 1.6 ± 0.3, respectively (Fig. 3A); the mean tumor volumes were 5.3 ± 1.6 mm^3, 5.5 ± 1.3 mm^3, and 4.6 ± 1.5 mm^3, respectively (Fig. 3B); and the mean tumor surface areas were 33.4 ± 9.7 mm^2, 37.1 ± 7.6 mm^2, and 28.6 ± 8.6 mm^2, respectively (Fig. 3C). For male *Dhh-Cre; Nf1*$^{R683X/4F}$ mice in the normal food control group, the mean tumor number, volume, and surface area of tumors per mouse were 2.7 ± 0.3, 5.8 ± 1.3 mm^3, and 39.1 ± 7.8 mm^2, respectively. Although many measurements of tumors from the ataluren treatment groups were lower than those in the normal food control group, 0.3% ataluren treatment had the most obvious reductions. However, these differences were not significant by one-way ANOVA analyses. The mean tumor number, volume, and surface area in mice on 0.3% ataluren treatment were reduced 40.7%, 20.6%, and 22.7%, respectively, compared to the comparable measurements in the control group. Although lacking statistical significance, these results suggested that ataluren may restrict tumor growth.

The results of dissection analyses were similar but were slightly more promising statistically. In female *Dhh-Cre; Nf1*$^{R683X/4F}$ mice on chow supplemented with 0.03%, 0.1%, and 0.3% ataluren, the mean tumor numbers were 4 ± 0.7, 6.7 ± 1.6, and 3.7 ± 0.9, respectively (Fig. 4B); the mean tumor diameters were 1.3 ± 0.06 mm, 1.3 ± 0.04 mm, and 1.3 ± 0.05 mm, respectively (Fig. 4C); and the mean tumor perimeters were 7.6 ± 0.4 mm, 7.6 ± 0.3 mm, and 7.5 ± 0.3 mm, respectively (Fig. 4D). There were no significant differences in these measurements from ataluren treated mice compared to those from mice on normal food (mean tumor number: 4.6 ± 0.1; mean tumor diameter: 1.4 ± 0.04 mm; and mean tumor perimeter: 7.7 ± 0.3 mm). In male *Dhh-Cre; Nf1*$^{R683X/4F}$ mice, the mean total tumor number in 0.1% ataluren treatment (1.5 ± 0.5 per mouse) or 0.3% ataluren treatment (1.6 ± 0.5 per mouse) was significantly lower than that in the normal food control (3.2 ± 0.4 per mouse) (Fig. 4B). However, no statistically significant effect was observed in the 0.03% ataluren treatment group (2.2 ± 0.5 per mouse). There was no significant reduction in mean tumor diameter between 0.03% ataluren treatment (1.4 ± 0.06 mm), 0.3% ataluren treatment (1.2 ± 0.05 mm), and the control group (1.2 ± 0.03 mm), but the mean diameter in the 0.1% ataluren treatment group (1.5 ± 0.09 mm) was significantly larger than that in the control group (Fig. 4C). The mean perimeter in 0.3% ataluren treatment (5.3 ± 0.4 mm) was significantly lower than in the control group (7.2 ± 0.3 mm), while no significant changes were observed in 0.03% ataluren treatment (7.5 ± 0.5 mm) and 0.1% ataluren treatment (8.9 ± 0.6 mm) (Fig. 4D). Our dissection results suggest that ataluren may restrict tumor growth in *Dhh-Cre; Nf1*$^{R683X/4F}$ male mice and the best treatment regimen was 0.3% ataluren delivered after weaning.

When evaluating the effects of ataluren on paralysis symptoms, we found fewer *Dhh-Cre; Nf1*$^{R683X/4F}$ male mice developed paralysis phenotypes by the end of 0.03% ataluren treatment (Fig. 6F; 10% developed paralysis: all in Paralysis II) and 0.3% ataluren treatment (Fig. 6H; 15.4% developed paralysis: 7.7% in Paralysis I, 7.7% in Paralysis II)

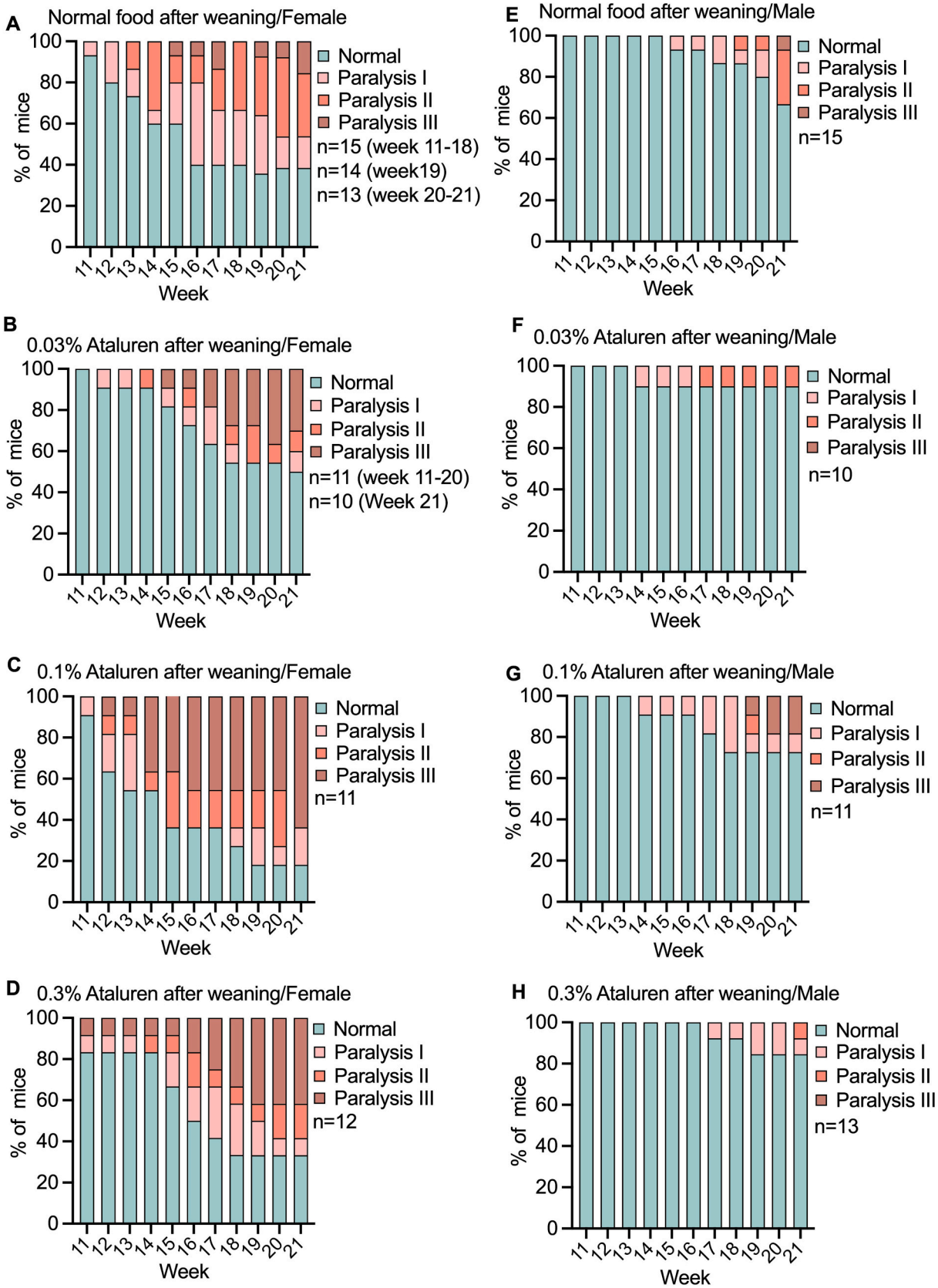


Fig. 6. Paralysis analyses of *Dhh-Cre; Nf1*$^{R683X/4F}$ mice on Regimen I. Percentage of mice with normal, Paralysis I, Paralysis II, or Paralysis III symptoms from the female and male mice kept on normal chow (A, E), 0.03% ataluren chow (B, F), 0.1% ataluren chow (C, G), and 0.3% ataluren chow (D, H).

compared to that of control *Dhh-Cre; Nf1*$^{R683X/4F}$ mice on normal food (Fig. 6E; 33.3% developed paralysis: 26.6% in Paralysis I, 6.7% in Paralysis III). The percentage of paralyzed mice on 0.1% ataluren treatment was also reduced, but to a lesser extent (Fig. 6G; 27.3% developed paralysis: 9.1% in Paralysis I, 18.2% in Paralysis III). We did not detect any improvement of paralysis phenotypes from female *Dhh-Cre; Nf1*$^{R683X/4F}$ mice on any level of ataluren chow by the end of our treatment. Instead, mice on 0.1% ataluren treatment showed more severe paralysis symptoms than controls (Figs. 6A-D, see week 21). However, we found that 0.03% ataluren treatment appeared to slow the development of paralysis at early ages, i.e., fewer mice developed paralysis phenotypes before week 17 (Figs. 6A and B, see weeks 11–16). There was no improvement of paralysis phenotypes in female mice on 0.1% and 0.3% ataluren at any age (Fig. 6C and D).

To test the nonsense suppressing effects of clitocine in *Dhh-Cre; Nf1*$^{R683X/4F}$ mice, male or female mice were injected with clitocine (1 mg/kg or 5 mg/kg) or PBS biweekly after weaning for five months (Fig. 1, Regimen II). Growth curves showed that the body weights of female or male *Dhh-Cre; Nf1*$^{R683X/4F}$ mice that received clitocine injections or the PBS control were similar (Fig. 2S, A). Tumor burden was analyzed by MRI. The mean total number from mice on PBS, 1 mg/kg clitocine, or 5 mg/kg clitocine injection was 3 ± 0.5, 3.7 ± 0.8, or 3.5 ± 0.7 in females, respectively, and was 1.3 ± 0.3, 3.5 ± 0.9, or 2.6 ± 1.0 in males, respectively (Fig. 3S1, A). The mean tumor volume from mice on PBS, 1 mg/kg clitocine, or 5 mg/kg clitocine injection was 7.5 ± 2.1 mm^3, 10 ± 2.3 mm^3, or 9.8 ± 3.1 mm^3, respectively, in females and was 3 ± 1.6 mm^3, 6.8 ± 2.4 mm^3, or 5.1 ± 1.6 mm^3, respectively, in males (Fig. 3S1, B). The mean tumor surface area from mice on PBS, 1 mg/kg clitocine, or 5 mg/kg clitocine injection was 48.4 ± 10.6 mm^2, 61.1 ± 13.0 mm^2, or 60.3 ± 17.5 mm^2, respectively, in females and was 19.4 ± 8.6 mm^2, 45.9 ± 15.3 mm^2, or 34.2 ± 11.1 mm^2, respectively, in males (Fig. 3S1, C). Clitocine injections resulted in increased levels of tumor burden, especially in male mice. Note, however, that the increases between different injection groups did not show significant differences. The lack of significance may be due to the small sample size, but the increased trends of measurements in neurofibromas upon clitocine injections suggest that clitocine is likely not functional in *Dhh-Cre; Nf1*$^{R683X/4F}$ mice.

Our data from mice on Regimen I and Regimen II indicate that: i) ataluren has some therapeutic effects restricting neurofibromas in male *Dhh-Cre; Nf1*$^{R683X/4F}$ mice and that 0.3% ataluren works better than the other two dosages, ii) ataluren can slow or alleviate paralysis symptoms in male mice by the end of treatment and in female mice at younger ages, but the optimal dosing was different in male and female mice, and iii) clitocine may increase the tumor burden in *Dhh-Cre; Nf1*$^{R683X/4F}$ mice.

2.3. Dosing schedule influences ataluren's effectiveness in Dhh-Cre; *Nf1*$^{R683X/4F}$ mice

To test whether ataluren administered at different ages has therapeutic effects, we analyzed *Dhh-Cre; Nf1*$^{R683X/4F}$ mice on Regimens III and IV in which they had been kept on normal chow for one or two months, respectively, and then switched to three levels of ataluren chow for four or three months (Fig. 1B, Regimens III and IV). Growth curves of these mice showed no significant differences between treatment groups in female or male *Dhh-Cre; Nf1*$^{R683X/4F}$ mice on Regimen III (Figs. 2S, B and C) or Regimen IV (Figs. 2S, D and E).

Volumetric MRI data from *Dhh-Cre; Nf1*$^{R683X/4F}$ mice on Regimen III showed that male and female mice on 0.1% ataluren treatment, but not the other two dosages, manifested decreased trends in tumor number, volume, and surface area compared to mice on normal chow (Figs. 3S2, A-C). Consistently, in females, fewer mice developed paralysis phenotypes (41.6% in the 0.1% ataluren treatment group vs. 61.5% in control group) by the end of treatment (Fig. 6S1, B, and Fig. 6A). In male mice, although the percentage of paralysis phenotypes was not reduced, mice had milder paralysis symptoms, with only the Paralysis I symptom observed in the 0.1% ataluren group compared to Paralysis II and III symptoms observed in the control group (Fig. 6S1, E, and Fig. 6E). There was no improvement of paralysis phenotypes from mice on 0.03% or 0.3% ataluren treatments (Figs. 6S1x, A, C, D, and F).

Volumetric analyses of mice on Regimen IV indicated that female mice on 0.03% ataluren and male mice on 0.3% ataluren had decreased trends in tumor number, volume, and surface area (Figs. 3S3, A-C, female group), and male mice on 0.03% ataluren showed slightly decreased trends in tumor volume and surface area, but not in tumor number (Figs. 3S3, A-C; male group). Development of paralysis symptoms was slowed by 0.03% ataluren treatment in female mice at early ages (Fig. 6S2, A, weeks 11–17), and by 0.03% ataluren and 0.3% ataluren treatment in male mice by the end of treatment (Figs. 6S2, D, F). There was no improvement observed in mice on other ataluren dosages (Figs. 6S2, B, C, E).

Collectively, these results suggest that mice of different sex and age require a distinct level of ataluren for treatment to be effective.

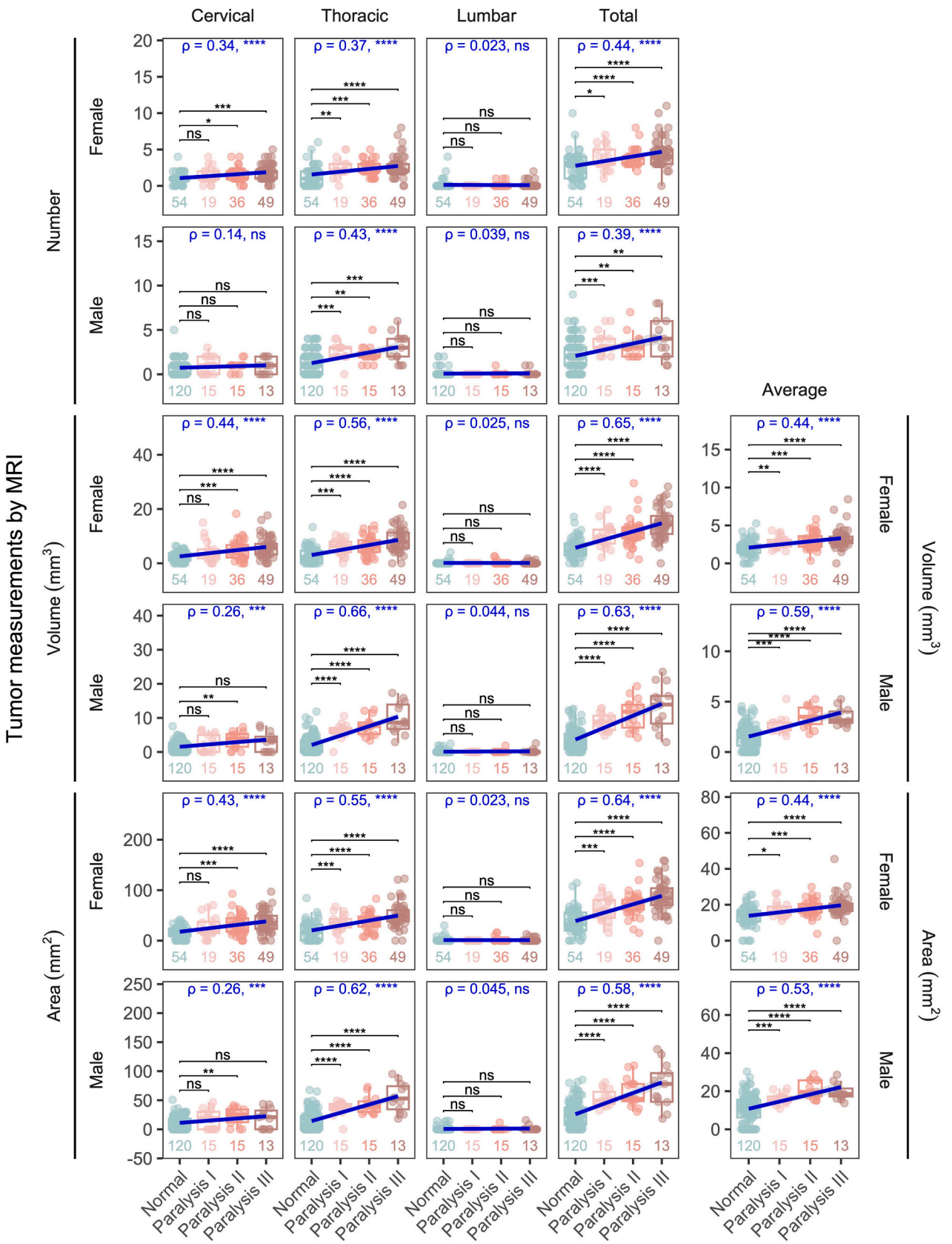
2.4. The severity of paralysis phenotypes reflects the extent of total tumor volume in Dhh-Cre; *Nf1*$^{R683X/4F}$ mice

The paralysis phenotype of *Nf1* mouse models has been reported to be correlated with neurofibromas formed along the spinal cord (Li et al., 2016; Wu et al., 2008). However, whether the severity of paralysis symptoms correlates with differences in total tumor numbers, tumor sizes, or tumor positions in mice still needs to be clarified. We pooled MRI data of male or female *Dhh-Cre; Nf1*$^{R683X/4F}$ mice from all treatment groups and used the Mann Whitney *U* test to compare differences between penetrance of paralysis phenotypes and MRI measurements of tumors (number, volume, and surface area of tumors formed in the cervical, thoracic, lumbar, and full spine, and also the average tumor volume/surface area in each mouse) (Fig. 7). We fit a line and calculated Spearman's correlation coefficient (labeled on each panel) for each comparison (Fig. 7). For all comparisons, the total tumor volume was strongly corelated with the degree of paralysis phenotypes with a Spearman's correlation coefficient of 0.65 in female mice and 0.63 in male mice. The change of severity of paralysis phenotypes was best reflected by the change in total tumor volume. Our analyses indicate that differences in total tumor volume in mice could be deduced from the penetrance of paralysis phenotypes.

Our analysis of paralysis phenotypes of female mice on Regimens I, III, and IV showed that different concentrations of ataluren treatment changed the progression of paralysis phenotypes at early ages (Figs. 6, 6S1, and 6S2), Hence, we pooled all the paralysis evaluations of female mice on Regimens I, III, and IV and performed regression analysis to estimate the contribution of treatments and age on the percentage of paralyzed female mice. As expected, on average, the percentage of paralyzed mice increased with age (i.e., there was a progressive increase in the percentage as weeks went by; Fig. 8, upper panel). We found that 0.03% ataluren in Regimen I, 0.1% ataluren in Regimen III, and 0.03% ataluren in Regimen IV significantly reduced the average percentage of paralyzed mice by 14–19%, while 0.1% ataluren in Regimen I, 0.3% ataluren in Regimen III, and 0.3% ataluren in Regimen IV significantly increased the average percentage of paralyzed mice by 6–13% (Fig. 8). Collectively, these data suggest that, when dosing appropriately, ataluren could slow the development of paralysis phenotypes and thus the growth of neurofibromas in *Dhh-Cre; Nf1*$^{R683X/4F}$ mice.

3. Discussion

Although NF1 is a monogenic genetic disease, the broad spectrum of its clinical manifestations and variabilities in disease presentations cannot be solely explained by pathologic variants in *NF1*. There is evidence suggesting that sex is also a risk factor affecting the development of NF1 symptoms and mortality. Several clinical and experimental studies have found that female NF1 patients and mouse models have a



(caption on next page)

Fig. 7. Paralysis phenotypes reflect total tumor volume in *Dhh-Cre; Nf1*$^{R683X/4F}$ mice. Comparison of tumor measurements by MRI among mice with different paralysis phenotypes. Tumor measurements included the total tumor number, volume, and surface area in the cervical spine, thoracic spine, lumbar spine, and full spine, as well as average tumor volume and surface area which were calculated by dividing the total volume and surface area by the number of tumors. The relationships between tumor measurements (y-axis) and final paralysis phenotypes (x-axis) were evaluated by two statistical approaches. First, unpaired two-tailed Mann Whitney *U* test with Benjamini-Hochberg method for multiple-testing correction was used to compare the distribution of a tumor measurement in each level of paralyzed mice (Paralysis I, II, or III) to that in non-paralyzed mice (Normal). Second, paralysis phenotypes were ranked by their severity (Normal = 1, Paralysis III = 4) and Spearman's correlation was used to determine whether a tumor feature significantly increases or decreases with the severity of paralysis phenotypes. Spearman's rank correlation (ρ) and the associated significance level are provided along with a linear regression trend line (blue). For both approaches, significance levels are indicated by the following: (ns) not significant, $^{*}p < 0.05$, $^{**}p < 0.01$, $^{***}p < 0.001$, $^{****}p < 0.0001$. The number of mice in each paralysis group is provided at the bottom. (For interpretation of the references to colour in this Fig. legend, the reader is referred to the web version of this article.)

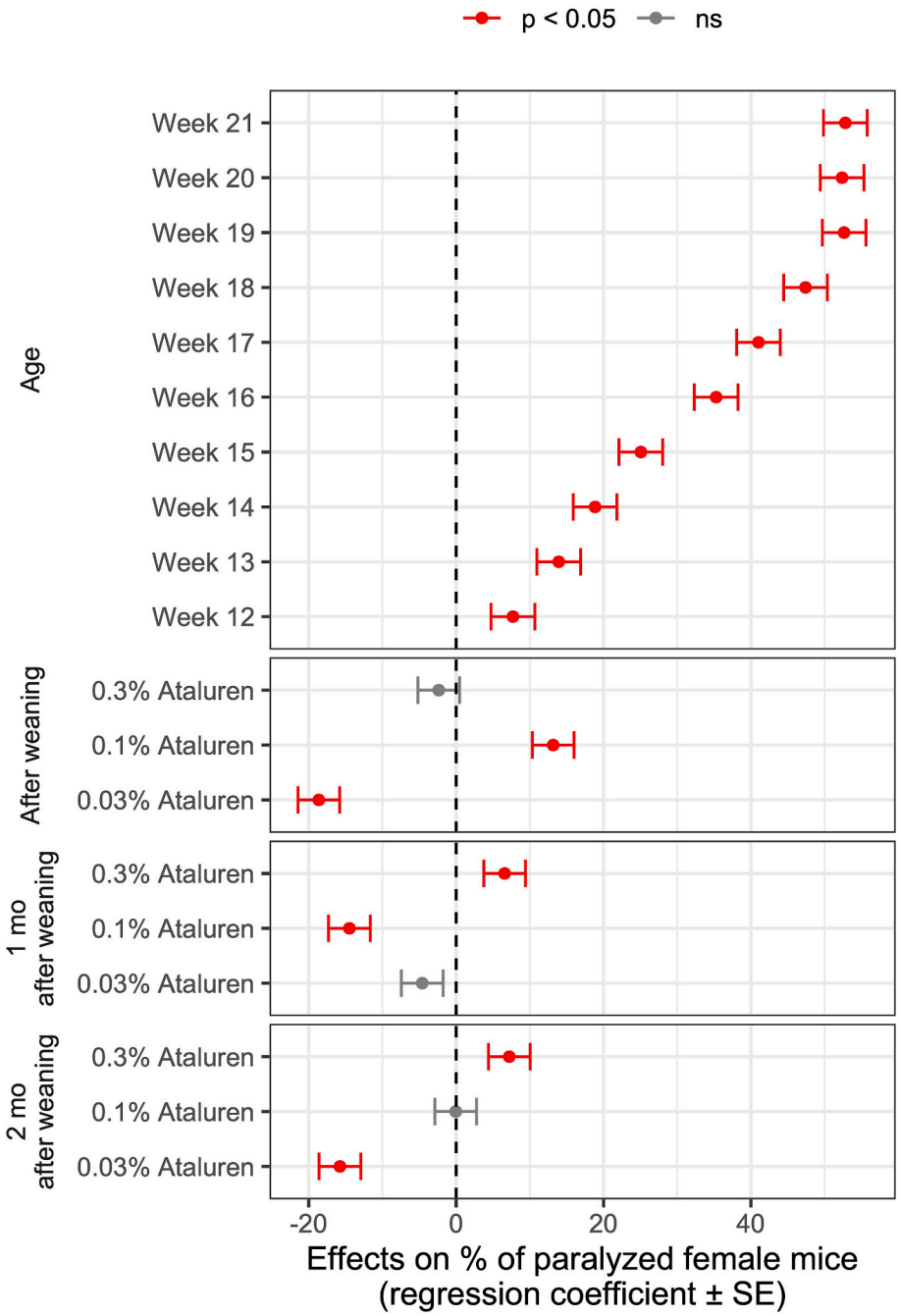


Fig. 8. Effects of ataluren treatment on paralysis phenotypes depends on ataluren dosage and age of mice. Linear regression was performed to assess how treatment regimens and developmental time (week) affected the percentage of paralyzed mice (female). Regression coefficient ± SE (x-axis) reflects the magnitude of effect of each variable (y-axis) on percentage of paralyzed mice (Red = significant, $p < 0.05$; Grey = not significant). A positive coefficient indicates an increase while a negative coefficient indicates a decrease in overall percentage of paralyzed mice. (For interpretation of the references to colour in this Fig. legend, the reader is referred to the web version of this article.)

higher prevalence of optic pathway gliomas (Diggs-Andrews et al., 2014; Henning et al., 2021; Robert-Boire et al., 2017; Toonen et al., 2017; Trevisson et al., 2017; Warrington et al., 2015) and a total population study of NF1 mortality in Finland indicates that women may have a higher excess NF1 mortality than men (Uusitalo et al., 2015). Other sex-related differences in cognitive, learning, and behavioral alterations have been observed (Chisholm et al., 2022; Coude et al., 2006; Gutierrez et al., 2023; Hyman et al., 2005; Santos et al., 2023). In this study, we have evaluated sex differences related to the growth of body weight, the formation of neurofibromas, and the development of paralysis phenotypes in a *Dhh-Cre; Nf1*$^{R683X/4F}$ mouse model that recapitulates human neurofibroma formation phenotypes. We observed that: i) male mice weighed less than their littermates while female mice did not (Figs. 2A and B) and ii) the development of neurofibromas and paralysis phenotypes were faster in female mice than in male mice (Figs. 3A-C, 4B and C, 6A and E). These results suggest that the presentation and development of PNFs in NF1 patients may also exhibit sex-related differences. PNFs are more likely to be correlated with functional deficits and malignant transformation (Friedrich et al., 2007; Mautner et al., 2006), so that sex factor in the development of PNFs needs to be validated in clinical studies, which may benefit selection of therapeutic treatments and prognosis.

Although paralysis symptoms have been reported in the *Dhh-Cre; Nf1*$^{R683X/4F}$ mouse model (Li et al., 2016), the correlation of paralysis with neurofibroma features has not been reported previously. Our study showed that the penetrance of paralysis phenotypes in the *Dhh-Cre; Nf1*$^{R683X/4F}$ mouse model reflects total tumor volume (Fig. 7). In addition to MRI and gross dissection measurements, this newly described analysis of the development of paralysis phenotypes in *Dhh-Cre; Nf1*$^{R683X/4F}$ mice provides an additional method to assess neurofibroma tumor burden (Figs. 5, 6, 6S1, 6S2). Since MRI quantitation requires more mice to compensate for the heterogeneity of neurofibromas to obtain statistical significance, while gross dissection of spinal cords is time consuming, paralysis analysis, although indirect, provides an alternative and perhaps more efficient method to reflect differences in tumor burden in *Dhh-Cre; Nf1*$^{R683X/4F}$ mice.

For NF1 patients with PNFs, surgical removal is still the optimal treatment, but this approach is not always feasible due to the locations of PNFs and the potential risks of surgery (Fisher et al., 2022). Likewise, a MEK1/2 inhibitor, selumetinib, has recently been approved by the FDA for the treatment of inoperable symptomatic PNFs in children, but the known and potentially unknown toxicities of this drug make its long-term use uncertain (Fisher et al., 2022; Mukhopadhyay et al., 2021). The nonsense suppression drug, ataluren, has an excellent safety record and has been shown to promote nonsense codon readthrough in *Nf1* nonsense-containing mouse embryonic stem cell derived neurons, cultured human cells, and patients (Bushby et al., 2014; Peltz et al., 2013; Welch et al., 2007; Wu et al., 2022). Thus, ataluren may be a potentially useful drug for NF1 patients with nonsense mutations. Here, we tested three levels of ataluren in an NF1 patient-derived nonsense mouse model following three treatment regimens (Fig. 1B, Regimens I, III, and IV). In Regimen I, we found that 0.03% ataluren in chow fed to females could slow the growth of neurofibromas at an early age while 0.3% ataluren in chow fed to male mice was optimal for reduced neurofibroma growth (Figs. 3, 4B, D, 6B, H, 8). These results in a mouse model indicate that ataluren may be applicable to NF1 nonsense mutation patients. Moreover, our results showing that female and male mice responded differently to ataluren is consistent with previous studies of gender differences in pharmacokinetics and pharmacodynamics revealing that women generally need lower drug dosages than men (Soldin and Mattison, 2009; Whitley and Lindsey, 2009; Zucker and Prendergast, 2020). Furthermore, our findings reinforce the notion that sex should be considered when assessing medical therapeutics for NF1 patients.

The results from mice on Regimen I, III, and IV showed that ataluren fed to mice at different ages affected the therapeutic outcomes. Feeding of 0.03% ataluren in female mice and 0.3% ataluren in male mice alleviated the neurofibroma or paralysis phenotypes in Regimen I and IV (Figs. 3, 4B, D, 6B, H, 8, 3S3, 6S2A, 6S2F), but had adverse effects in Regimen III (Figs. 3S2, 6S1A, 6S1F), whereas 0.1% ataluren alleviated some symptoms in Regimen III (Figs. 3S2, 6S1B, 6S1E). These results suggest that adjusting treatment schedules according to age may yield better outcomes. The results of different optimal dosages between treatment regimens also provide a hint that NF1 patients enrolled at different ages may need adjusted drug dosages to get the best responses in clinical studies.

Our results indicate that ataluren may be a promising treatment for nonsense mutation *NF1* patients, but that further studies are required to consolidate our findings. For example, some of our results lack statistical significance, in part due to the heterogeneity of neurofibromas in this model. This suggests that larger sample sizes should be included in future studies or new methods used in quantitation of tumor burden. Our study may also have limited the expected efficacy of ataluren since the mouse model employed contains only one suppressible nonsense allele. Finally, in light of the results presented here, ataluren dosages employed in future studies need to take into account the pertinent sex and age factors we observed.

4. Materials and methods

4.1. Animals

An animal study protocol (A-2663-19) was approved by the Institutional Animal Care and Use Committee (IACUC) at UMass Chan Medical School. All animals were housed in a vivarium with free access to chow and water on a 12-h light/dark cycle with routine care from animal care technicians and veterinarians. The *Dhh-Cre; Nf1*$^{R683X/4F}$ plexiform neurofibroma mouse model was described previously (Li et al., 2016). *Nf1*$^{R683X/4F}$ mice were a gift from Dr. Robert Kesterson at the Heersink School of Medicine of the University of Alabama at Birmingham. *Dhh-Cre* mice were obtained from the Jackson Laboratory (stock #012929). To generate the desired genotype, female *Dhh-Cre* mice were bred with male *Nf1*$^{R683X/4F}$ mice to obtain female *Dhh-Cre*; *Nf1*$^{R683X/+}$ F1 mice. Then, female *Dhh-Cre*; *Nf1*$^{R683X/+}$ mice were bred with male *Nf1*$^{R683X/4F}$ mice to generate the experimental *Dhh-Cre; Nf1*$^{R683X/4F}$ F2 mice and the sibling control mice. Once a week, we monitored and recorded body weights and paralysis phenotypes of these mice fed with normal or ataluren infused chow (ataluren was provided by PTC Therapeutics, Inc. and the ataluren infused chows were made by Research Diets, Inc.). Mice were genotyped by PCR using the following primer pairs: *Dhh-Cre* line: forward-5' CCTTCTCTATCTGCGGTGCT, reverse-5' ACGGACA-GAAGCATTTTCCA; *Nf1*^{4F} allele: forward-5' GAGTTGGGAA-GAATGGTGTAGTGC, reverse-5' ACCTCTGGAAGAACAGTTGGCG; *Nf1*^{R683X} allele: forward-5' TGATTATTTGACCGTGTGGC, reverse-5' ACTGACTGAAACAATGACCC.

4.2. Tumor volumetric analysis

MRI was performed using a 3T system (Philips Ingenia 3T, Philips Healthcare). A 40-mm in-house built coil was used as the radiofrequency transmitter and receiver to scan the mice, covering the entire spinal cord from the cervical to thoracic to lumbar regions. Mice were anesthetized using 1–2% isoflurane in an oxygen/air mixture through a vaporizer, with body temperature maintained by a heating pad and respiration rate monitored using a physiological monitoring system. Images were acquired using a 3D T2-weighted turbo spin echo sequence with the following parameters: repetition time = 2000 ms, echo time = 80 ms, flip angle = 90°, slice thickness = 0.25 mm, field of view = 240 mm × 222 mm, reconstructed matrix size = 288 × 288, number of average = 1, and acquisition time = ~30 mins. All mice survived the entire duration of imaging time. For image analysis, the T2-weighted images were reconstructed into a 3D volume colormap using AMIRA (V6.0.1, Thermo

Fisher Scientific, Waltham, MA, USA). The neurofibromas were identified based on pixel intensity and/or morphological changes surrounding the DRGs and/or nerve roots. The neurofibromas were then segmented on the 2D slices, reconstructed into 3D volumes, and then the number, surface area, and volume of tumors were calculated.

4.3. Mouse dissection and tumor burden analysis

Mice were euthanized by carbon dioxide inhalation and perfused intracardially with phosphate buffered saline followed by 4% paraformaldehyde, and preserved in 10% neutral buffered formalin (Epredia #5725). Before dissection, mice were soaked overnight in decalcification solution (Epredia #5501), then transferred to phosphate buffered saline. The intact spinal cord with attached nerve roots was dissected out in a fume hood under a stereo zoom microscope (Wild Heerbrugg, model M5). A tumor was defined as a mass surrounding the nerve root/DRG with a diameter >1 mm. The diameter and perimeter of a tumor was measured by ImageJ. The tumor numbers, diameters and perimeters per mouse were compared between different groups.

4.4. Statistical analysis

Statistical analyses and graphs were generated with GraphPad Prism (version 9) or R (version 4.2.0). The comparisons were analyzed by unpaired two-tailed Student's *t*-test with Welch's correction for two independent groups, unpaired two-tailed Mann Whitney *U* test with Benjamini-Hochberg method for multiple-testing correction, one-way ANOVA with Dunnett's correction for multiple groups, or two-way ANOVA with Tukey's multiple comparisons correction. *P* values showing significance were indicated by asterisks as follows: *, $p < 0.05$; **, $p < 0.01$; ***, $p < 0.001$, ****, $p < 0.0001$. Graphs were presented as mean ± SEM or mean ± SD.

0.03% ataluren chow ($n = 10$), 0.1% ataluren chow (n = 11), 0.3% ataluren chow ($n = 13$), and siblings on normal chow ($n = 5$). Body weights were measured weekly. Data are presented as mean ± SD. Ordinary one-way ANOVA with Dunnett's test was used to identify significant pairs between different groups in both male and female mice. Body weights of the male *Dhh-Cre; Nf1*$^{R683X/4F}$ mice on normal chow are significantly lighter than those of their WT sibling littermates, $p = 0.0003$.

Supplementary data to this article can be found online at https://doi.org/10.1016/j.expneurol.2024.114914.

CRediT authorship contribution statement

Chan Wu: Conceptualization, Supervision, Investigation, Methodology, Data curation, Formal analysis, Writing – original draft, Writing – review & editing. **Mohammed Salman Shazeeb:** Investigation, Formal analysis, Resources, Writing – review & editing. **Kotchaphorn Mangkalaphiban:** Formal analysis, Writing – review & editing. **George Han:** Investigation. **Ahmet Peker:** Investigation. **Zubir S. Rentiya:** Investigation. **Matthew J. Gounis:** Conceptualization, Resources, Funding acquisition. **Allan Jacobson:** Conceptualization, Supervision, Methodology, Resources, Funding acquisition, Writing – review & editing.

Declaration of competing interest

A.J. is co-founder, director, consultant and shareholder for PTC Therapeutics Inc. M.J.G. is a consultant for Alembic LLC, Astrocyte Pharmaceuticals, BendIt Technologies, Cerenovus, Imperative Care, Jacob's Institute, Medtronic Neurovascular, Mivi Neurosciences, phenox GMbH, Q'Apel, Route 92 Medical, Scientia, Simcerre, Stryker Neurovascular, Stryker Sustainability Solutions, and Wallaby Medical and shareholder of Imperative Care, InNeuroCo, Galaxy Therapeutics, Kapto, Neurogami and Synchron. M.S.S. is a consultant for Sanofi. All other authors declare no competing interests.

Data availability

No data was used for the research described in the article.

Acknowledgments

This work was supported by grants to A.J. (616394) and to M.J.G. and Miguel Esteves (563749) from the Gilbert Family Foundation. We thank: PTC Therapeutics Inc. for providing ataluren and for facilitating access to ataluren infused chows; the UMass Chan Image Processing and Analysis Core (iPAC) for computing resources; Marla Weetall and Xin Zhao for helpful discussions; Viraj Moholkar and Aditya Joshi for their help with image analyses; and Drs. Robert King and Shaokuan Zheng (Advanced MRI Center at UMass Chan) for their technical support with the imaging experiments.

References

Anastasaki, C., Morris, S.M., Gao, F., Gutmann, D.H., 2017. Children with 5′-end NF1 gene mutations are more likely to have glioma. Neurol. Genet. 3, e192.
Bashyam, M.D., 2009. Nonsense-mediated decay: linking a basic cellular process to human disease. Expert. Rev. Mol. Diagn. 9, 299–303.
Brinckmann, A., Mischung, C., Bassmann, I., Kuhnisch, J., Schuelke, M., Tinschert, S., Nurnberg, P., 2007. Detection of novel NF1 mutations and rapid mutation prescreening with pyrosequencing. Electrophoresis 28, 4295–4301.
Bushby, K., Finkel, R., Wong, B., Barohn, R., Campbell, C., Comi, G.P., Connolly, A.M., Day, J.W., Flanigan, K.M., Goemans, N., et al., 2014. Ataluren treatment of patients with nonsense mutation dystrophinopathy. Muscle Nerve 50, 477–487.
Chisholm, A.K., Lami, F., Haebich, K.M., Ure, A., Brignell, A., Maloof, T., Pride, N.A., Walsh, K.S., Maier, A., Rouel, M., et al., 2022. Sex- and age-related differences in autistic behaviours in children with neurofibromatosis type 1. J. Autism Dev. Disord. 53 (7), 2835–2850.
Cimino, P.J., Gutmann, D.H., 2018. Neurofibromatosis type 1. Handb. Clin. Neurol. 148, 799–811.
Coude, F.X., Mignot, C., Lyonnet, S., Munnich, A., 2006. Academic impairment is the most frequent complication of neurofibromatosis type-1 (NF1) in children. Behav. Genet. 36, 660–664.
DeClue, J.E., Cohen, B.D., Lowy, D.R., 1991. Identification and characterization of the neurofibromatosis type 1 protein product. Proc. Natl. Acad. Sci. USA 88, 9914–9918.
Diggs-Andrews, K.A., Brown, J.A., Gianino, S.M., Rubin, J.B., Wozniak, D.F., Gutmann, D.H., 2014. Sex is a major determinant of neuronal dysfunction in neurofibromatosis type 1. Ann. Neurol. 75, 309–316.
Evans, D.G., Baser, M.E., McGaughran, J., Sharif, S., Howard, E., Moran, A., 2002. Malignant peripheral nerve sheath tumours in neurofibromatosis 1. J. Med. Genet. 39, 311–314.
Fisher, M.J., Blakeley, J.O., Weiss, B.D., Dombi, E., Ahlawat, S., Akshintala, S., Belzberg, A.J., Bornhorst, M., Bredella, M.A., Cai, W., et al., 2022. Management of neurofibromatosis type 1-associated plexiform neurofibromas. Neuro-Oncology 24, 1827–1844.
Friedman, J.M., 1999. Epidemiology of neurofibromatosis type 1. Am. J. Med. Genet. 89, 1–6.
Friedrich, R.E., Hartmann, M., Mautner, V.F., 2007. Malignant peripheral nerve sheath tumors (MPNST) in NF1-affected children. Anticancer Res. 27, 1957–1960.
Friesen, W.J., Trotta, C.R., Tomizawa, Y., Zhuo, J., Johnson, B., Sierra, J., Roy, B., Weetall, M., Hedrick, J., Sheedy, J., et al., 2017. The nucleoside analog clitocine is a potent and efficacious readthrough agent. RNA 23, 567–577.
Gross, A.M., Singh, G., Akshintala, S., Baldwin, A., Dombi, E., Ukwuani, S., Goodwin, A., Liewehr, D.J., Steinberg, S.M., Widemann, B.C., 2018. Association of plexiform neurofibroma volume changes and development of clinical morbidities in neurofibromatosis 1. Neuro-Oncology 20, 1643–1651.
Gutierrez, W.R., Rytlewski, J.D., Scherer, A., Roughton, G.A., Carnevale, N.C., Vyas, K.Y., McGivney, G.R., Brockman, Q.R., Knepper-Adrian, V., Dodd, R.D., 2023. Loss of Nf1 and Ink4a/Arf are associated with sex-dependent growth differences in a mouse model of embryonal rhabdomyosarcoma. Curr. Issues Mol. Biol. 45, 1218–1232.
Gutmann, D.H., Wood, D.L., Collins, F.S., 1991. Identification of the neurofibromatosis type 1 gene product. Proc. Natl. Acad. Sci. USA 88, 9658–9662.
Gutmann, D.H., Ferner, R.E., Listernick, R.H., Korf, B.R., Wolters, P.L., Johnson, K.J., 2017. Neurofibromatosis type 1. Nat. Rev. Dis. Primers 3, 17004.
He, F., Jacobson, A., 2015. Nonsense-mediated mRNA decay: degradation of defective transcripts is only part of the story. Annu. Rev. Genet. 49, 339–366.
Henning, A.M., Handrup, M.M., Kjeldsen, S.M., Larsen, D.A., Ejerskov, C., 2021. Optic pathway glioma and the sex association in neurofibromatosis type 1: a single-center study. Orphanet J. Rare Dis. 16, 489.
Hyman, S.L., Shores, A., North, K.N., 2005. The nature and frequency of cognitive deficits in children with neurofibromatosis type 1. Neurology 65, 1037–1044.
Keeling, K.M., Xue, X., Gunn, G., Bedwell, D.M., 2014. Therapeutics based on stop codon readthrough. Annu. Rev. Genomics Hum. Genet. 15, 371–394.

Leier, A., Bedwell, D.M., Chen, A.T., Dickson, G., Keeling, K.M., Kesterson, R.A., Korf, B. R., Marquez Lago, T.T., Muller, U.F., Popplewell, L., et al., 2020. Mutation-directed therapeutics for Neurofibromatosis type I. Mol. Ther. Nucleic Acids 20, 739–753.
Li, K., Turner, A.N., Chen, M., Brosius, S.N., Schoeb, T.R., Messiaen, L.M., Bedwell, D.M., Zinn, K.R., Anastasaki, C., Gutmann, D.H., et al., 2016. Mice with missense and nonsense NF1 mutations display divergent phenotypes compared with human neurofibromatosis type I. Dis. Model. Mech. 9, 759–767.
Mautner, V.F., Hartmann, M., Kluwe, L., Friedrich, R.E., Funsterer, C., 2006. MRI growth patterns of plexiform neurofibromas in patients with neurofibromatosis type 1. Neuroradiology 48, 160–165.
Mautner, V.F., Asuagbor, F.A., Dombi, E., Funsterer, C., Kluwe, L., Wenzel, R., Widemann, B.C., Friedman, J.M., 2008. Assessment of benign tumor burden by whole-body MRI in patients with neurofibromatosis 1. Neuro-Oncology 10, 593–598.
McDonald, C.M., Henricson, E.K., Abresch, R.T., Florence, J.M., Eagle, M., Gappmaier, E., Glanzman, A.M., Group PG-DS, Spiegel, R., Barth, J., et al., 2013. The 6-minute walk test and other endpoints in Duchenne muscular dystrophy: longitudinal natural history observations over 48 weeks from a multicenter study. Muscle Nerve 48, 343–356.
McDonald, C.M., Campbell, C., Torricelli, R.E., Finkel, R.S., Flanigan, K.M., Goemans, N., Heydemann, P., Kaminska, A., Kirschner, J., Muntoni, F., et al., 2017. Ataluren in patients with nonsense mutation Duchenne muscular dystrophy (ACT DMD): a multicentre, randomised, double-blind, placebo-controlled, phase 3 trial. Lancet 390, 1489–1498.
Mercuri, E., Osorio, A.N., Muntoni, F., Buccella, F., Desguerre, I., Kirschner, J., Tulinius, M., de Resende, M.B.D., Morgenroth, L.P., Gordish-Dressman, H., et al., 2023. Safety and effectiveness of ataluren in patients with nonsense mutation DMD in the STRIDE registry compared with the CINRG Duchenne natural history study (2015-2022): 2022 interim analysis. J. Neurol. 270, 3896–3913.
Miller, J.N., Pearce, D.A., 2014. Nonsense-mediated decay in genetic disease: friend or foe? Mutat. Res. 762, 52–64.
Mukhopadhyay, S., Maitra, A., Choudhury, S., 2021. Selumetinib: the first ever approved drug for neurofibromatosis-1 related inoperable plexiform neurofibroma. Curr. Med. Res. Opin. 37, 789–794.
Osborn, M.J., Upadhyaya, M., 1999. Evaluation of the protein truncation test and mutation detection in the NF1 gene: mutational analysis of 15 known and 40 unknown mutations. Hum. Genet. 105, 327–332.
Peltz, S.W., Welch, E.M., Jacobson, A., Trotta, C.R., Naryshkin, N., Sweeney, H.L., Bedwell, D.M., 2009. Nonsense suppression activity of PTC124 (ataluren). Proc. Natl. Acad. Sci. USA 106, E64 (author reply E65).
Peltz, S.W., Morsy, M., Welch, E.M., Jacobson, A., 2013. Ataluren as an agent for therapeutic nonsense suppression. Annu. Rev. Med. 64, 407–425.
Philpott, C., Tovell, H., Frayling, I.M., Cooper, D.N., Upadhyaya, M., 2017. The NF1 somatic mutational landscape in sporadic human cancers. Hum. Genom. 11, 13.
Plotkin, S.R., Bredella, M.A., Cai, W., Kassarjian, A., Harris, G.J., Esparza, S., Merker, V. L., Munn, L.L., Muzikansky, A., Askenazi, M., et al., 2012. Quantitative assessment of whole-body tumor burden in adult patients with neurofibromatosis. PLoS One 7, e35711.
Prada, C.E., Rangwala, F.A., Martin, L.J., Lovell, A.M., Saal, H.M., Schorry, E.K., Hopkin, R.J., 2012. Pediatric plexiform neurofibromas: impact on morbidity and mortality in neurofibromatosis type 1. J. Pediatr. 160, 461–467.
Rasmussen, S.A., Friedman, J.M., 2000. NF1 gene and neurofibromatosis 1. Am. J. Epidemiol. 151, 33–40.
Robert-Boire, V., Rosca, L., Samson, Y., Ospina, L.H., Perreault, S., 2017. Clinical presentation and outcome of patients with optic pathway glioma. Pediatr. Neurol. 75, 55–60.
Roy, B., Leszyk, J.D., Mangus, D.A., Jacobson, A., 2015. Nonsense suppression by near cognate tRNAs employs alternative base-pairing at codon positions 1 and 3. Proc. Natl. Acad. Sci. USA 112, 3038–3043.
Roy, B., Friesen, W.J., Tomizawa, Y., Leszyk, J.D., Zhuo, J., Johnson, B., Dakka, J., Trotta, C.R., Xue, X., Mutyam, V., et al., 2016. Ataluren stimulates ribosomal selection of near-cognate tRNAs to promote nonsense suppression. Proc. Natl. Acad. Sci. USA 113, 12508–12513.
Santos, S., Martins, B., Sereno, J., Martins, J., Castelo-Branco, M., Goncalves, J., 2023. Neurobehavioral sex-related differences in Nf1(+/−) mice: female show a "camouflaging"-type behavior. Biol. Sex Differ. 14, 24.
Soldin, O.P., Mattison, D.R., 2009. Sex differences in pharmacokinetics and pharmacodynamics. Clin. Pharmacokinet. 48, 143–157.
Stenson, P.D., Mort, M., Ball, E.V., Chapman, M., Evans, K., Azevedo, L., Hayden, M., Heywood, S., Millar, D.S., Phillips, A.D., Cooper, D.N., 2020. The human gene mutation database (HGMD((R))): optimizing its use in a clinical diagnostic or research setting. Hum. Genet. 139, 1197–1207.
Toonen, J.A., Solga, A.C., Ma, Y., Gutmann, D.H., 2017. Estrogen activation of microglia underlies the sexually dimorphic differences in Nf1 optic glioma-induced retinal pathology. J. Exp. Med. 214, 17–25.
Trevisson, E., Cassina, M., Opocher, E., Vicenzi, V., Lucchetta, M., Parrozzani, R., Miglionico, G., Mardari, R., Viscardi, E., Midena, E., Clementi, M., 2017. Natural history of optic pathway gliomas in a cohort of unselected patients affected by Neurofibromatosis 1. J. Neuro-Oncol. 134, 279–287.
Uusitalo, E., Leppavirta, J., Koffert, A., Suominen, S., Vahtera, J., Vahlberg, T., Poyhonen, M., Peltonen, J., Peltonen, S., 2015. Incidence and mortality of neurofibromatosis: a total population study in Finland. J. Invest. Dermatol. 135, 904–906.
Warrington, N.M., Sun, T., Luo, J., McKinstry, R.C., Parkin, P.C., Ganzhorn, S., Spoljaric, D., Albers, A.C., Merkelson, A., Stewart, D.R., et al., 2015. The cyclic AMP pathway is a sex-specific modifier of glioma risk in type I neurofibromatosis patients. Cancer Res. 75, 16–21.
Welch, E.M., Barton, E.R., Zhuo, J., Tomizawa, Y., Friesen, W.J., Trifillis, P., Paushkin, S., Patel, M., Trotta, C.R., Hwang, S., et al., 2007. PTC124 targets genetic disorders caused by nonsense mutations. Nature 447, 87–91.
Whitley, H., Lindsey, W., 2009. Sex-based differences in drug activity. Am. Fam. Physician 80, 1254–1258.
Wu, J., Williams, J.P., Rizvi, T.A., Kordich, J.J., Witte, D., Meijer, D., Stemmer-Rachamimov, A.O., Cancelas, J.A., Ratner, N., 2008. Plexiform and dermal neurofibromas and pigmentation are caused by Nf1 loss in desert hedgehog-expressing cells. Cancer Cell 13, 105–116.
Wu, C., Iyer, S., Wolfe, S.A., Jacobson, A., 2022. Functional restoration of mouse Nf1 nonsense alleles in differentiated cultured neurons. J. Hum. Genet. 67, 661–668.
Xu, G.F., O'Connell, P., Viskochil, D., Cawthon, R., Robertson, M., Culver, M., Dunn, D., Stevens, J., Gesteland, R., White, R., et al., 1990. The neurofibromatosis type 1 gene encodes a protein related to GAP. Cell 62, 599–608.
Zucker, I., Prendergast, B.J., 2020. Sex differences in pharmacokinetics predict adverse drug reactions in women. Biol. Sex Differ. 11, 32.